A nanoplasmonic probe for near-field imaging

J. A. J. Backs, S. Sederberg, and A. Y. Elezzabi*

Ultrafast Optics and Nanophotonics Laboratory, Department of Electrical and Computer Engineering, University of Alberta, Edmonton, Alberta T6G 2V4, Canada
**elezzabi@ece.ualberta.ca*

Abstract: We demonstrate a nanoplasmonic probe that incorporates a subwavelength aperture coupled to a fine probing tip. This probe is used in a hybrid near-field scanning optical microscope and atomic force microscope system that can simultaneously map the optical near-field and the topography of nanostructures. By spatially isolating but optically coupling the aperture and the localizing point, we obtained near-field images at a resolution of 45 nm, corresponding to $\lambda/14$. This nanoplasmonic probe design overcomes the resolution challenges of conventional apertured near-field optical probes and can provide substantially higher resolution than demonstrated in this work.

OCIS codes: (180.4243) Near-field microscopy; (240.6680) Surface plasmons; (260.3910) Metal optics; (310.6628) Subwavelength structures.

References and links

1. R. Zia, J. Schuller, and M. Brongersma, "Near-field characterization of guided polariton propagation and cutoff in surface plasmon waveguides," Phys. Rev. B **74**(16), 165415 (2006).
2. M. H. Chowdhury, J. M. Catchmark, and J. R. Lakowicz, "Imaging three-dimensional light propagation through periodic nanohole arrays using scanning aperture microscopy," Appl. Phys. Lett. **91**(10), 103118 (2007).
3. E. X. Jin and X. Xu, "Enhanced optical near field from a bowtie aperture," Appl. Phys. Lett. **88**(15), 153110 (2006).
4. R. Guo, E. C. Kinzel, Y. Li, S. M. Uppuluri, A. Raman, and X. Xu, "Three-dimensional mapping of optical near field of a nanoscale bowtie antenna," Opt. Express **18**(5), 4961–4971 (2010).
5. N. F. van Hulst, M. H. P. Moers, O. F. J. Noordman, R. G. Tack, F. B. Segerink, and B. Bölger, "Near-field optical microscope using a silicon-nitride probe," Appl. Phys. Lett. **62**(5), 461–463 (1993).
6. B. Hecht, B. Sick, U. P. Wild, V. Deckert, R. Zenobi, O. J. F. Martin, and D. W. Pohl, "Scanning near-field optical microscopy with aperture probes: fundamentals and applications," J. Chem. Phys. **112**(18), 7761–7774 (2000).
7. A. Jauß, J. Koenen, K. Weishaupt, and O. Hollricher, "Scanning near-field optical microscopy in life science," Single Mol. **3**(4), 232–235 (2002).
8. J. W. Kingsley, S. K. Ray, A. M. Adawi, G. J. Leggett, and D. G. Lidzey, "Optical nanolithography using a scanning near-field probe with an integrated light source," Appl. Phys. Lett. **93**(21), 213103 (2008).
9. M. Celebrano, P. Biagioni, M. Zavelani-Rossi, D. Polli, M. Labardi, M. Allegrini, M. Finazzi, L. Duò, and G. Cerullo, "Hollow-pyramid based scanning near-field optical microscope coupled to femtosecond pulses: a tool for nonlinear optics at the nanoscale," Rev. Sci. Instrum. **80**(3), 033704 (2009).
10. P. Biagioni, M. Celebrano, M. Zavelani-Rossi, D. Polli, M. Labardi, G. Lanzani, G. Cerullo, M. Finazzi, and L. Duò, "High-resolution imaging of local oxidation in polyfluorene thin films by nonlinear near-field microscopy," Appl. Phys. Lett. **91**(19), 191118 (2007).
11. S. Chen, H. Hsiung, W. Su, and D. Tsai, "Convenient near-field optical measurement and analysis of polystyrene spheres," Vacuum **81**(1), 129–132 (2006).
12. R. M. Stöckle, N. Schaller, V. Deckert, C. Fokas, and R. Zenobi, "Brighter near-field optical probes by means of improving the optical destruction threshold," J. Microsc. **194**(2-3), 378–382 (1999).
13. A. Dechant, S. K. Dew, S. E. Irvine, and A. Y. Elezzabi, "High-transmission solid-immersion apertured optical probes for near-field scanning optical microscopy," Appl. Phys. Lett. **86**(1), 013102 (2005).
14. H. Bethe, "Theory of diffraction by small holes," Phys. Rev. **66**(7-8), 163–182 (1944).
15. R. Vogelgesang, J. Dorfmüller, R. Esteban, R. T. Weitz, A. Dmitriev, and K. Kern, "Plasmonic nanostructures in aperture-less scanning near-field optical microscopy (aSNOM)," Phys. Status Solidi B **245**(10), 2255–2260 (2008).
16. Y. Zou and K. B. Crozier, "Experimental measurement of surface plasmon resonance of pyramidal metal nanoparticle tips," Proc. SPIE **7033**, 70331X (2008).
17. A. Naber, D. Molenda, U. C. Fischer, H.-J. Maas, C. Höppener, N. Lu, and H. Fuchs, "Enhanced light confinement in a near-field optical probe with a triangular aperture," Phys. Rev. Lett. **89**(21), 210801 (2002).
18. M. Specht, J. D. Pedarnig, W. M. Heckl, and T. W. Hänsch, "Scanning plasmon near-field microscope," Phys. Rev. Lett. **68**(4), 476–479 (1992).

#145386 - $15.00 USD Received 5 Apr 2011; revised 13 May 2011; accepted 22 May 2011; published 25 May 2011

19. F. Zenhausern, Y. Martin, and H. K. Wickramasinghe, "Scanning interferometric apertureless microscopy: optical imaging at 10 angstrom resolution," Science **269**(5227), 1083–1085 (1995).
20. Y. Inouye and S. Kawata, "Near-field scanning optical microscope with a metallic probe tip," Opt. Lett. **19**(3), 159–161 (1994).
21. R. Esteban, R. Vogelgesang, and K. Kern, "Full simulations of the apertureless scanning near field optical microscopy signal: achievable resolution and contrast," Opt. Express **17**(4), 2518–2529 (2009).
22. M. C. Quong and A. Y. Elezzabi, "Offset-apertured near-field scanning optical microscope probes," Opt. Express **15**(16), 10163–10174 (2007).
23. In particular, our nanoplasmonic probe had an imperfectly pyramidal tip (Fig. 3), a gold coating, and a large aperture, while the numerically-studied probe [22] had a perfectly conical tip, a metal coating of different thickness and material (silver), a different cantilever thickness, and a smaller cone angle. These differences preclude any quantitative comparison between the optical properties of the two probes.
24. R. Qiang, R. Chen, and J. Chen, "Modeling electrical properties of gold films at infrared frequency using FDTD method," Int. J. Infrared Millim. Waves **25**(8), 1263–1270 (2004).
25. M. Yan and M. Qiu, "Guided plasmon polariton at 2D metal corners," J. Opt. Soc. Am. B **24**(9), 2333–2342 (2007).

1. Introduction

The resolution of traditional optical microscopy systems is limited by the diffraction of light, but near-field scanning optical microscopy (NSOM) systems permit sub-diffraction mapping of electromagnetic energy distributions on nanostructures. In NSOM, a probe designed to focus electromagnetic energy to a sub-diffraction scale is brought close to a nanostructure. The interaction of the structure and the probe causes optical energy to scatter into the far-field where it can be detected. This highly localized electromagnetic interaction has found a variety of applications, such as the direct observation of surface plasmon (SP) waves [1] and near-field transmission patterns for nano-scale apertures [2–4]. Other examples include the characterization of optical thin films [5] and absorptive [5] or fluorescent [6,7] imaging of biological molecules. Optical nano-machining is also possible by highly localized optical ablation with a reported full-width at half maximum (FWHM) size of 70 nm in one example [6]. Nano-lithography in photo-sensitive films has been reported with a FWHM size of 35 nm using ultra-violet light [8]. Time-resolved and non-linear optical experiments have also been demonstrated [9,10].

A common NSOM method employs a metal-coated tapered optical fiber having a small aperture at its apex for delivering the localized electromagnetic energy [6,11]. However, these probes suffer from a low optical throughput and are easily damaged at moderate optical powers [12]. Greater durability and higher optical throughput has been achieved with hollow [3,4,9,10] and solid-immersion [13] pyramid-shaped apertured probes, but the spatial resolution is limited by the dimension of the aperture at the hollow pyramid's apex. Furthermore, the Bethe limit [14] requires that the optical throughput decreases with the fourth power of the aperture diameter, thus creating a trade-off between spatial resolution and contrast. Other techniques involve apertureless (scattering) probes, which provide enhanced spatial resolution capabilities [15,16]. While resolutions for apertured probes commonly range between 50 and 100 nm [6,10] and have been reported below 40 nm [17], apertureless techniques have approached single-nanometer resolution [18,19]. Generally, a disadvantage of apertureless techniques is the requirement for more sophisticated equipment (such as lock-in amplifiers [20,21] and interferometric setups [19]) to differentiate the scattered near-field optical signal from significant background light.

A hybrid nanoplasmonic probe design has recently been proposed wherein the optical aperture and the localizing structure (the probe tip) are spatially isolated from each other but nonetheless optically coupled such that optical energy is transported via SP waves between the aperture and the tip [22]. Numerical simulations showed that this design simultaneously provides the superior optical throughput of a large-diameter aperture along with the apex-limited resolution of an apertureless probe.

In this paper, we demonstrate near-field optical imaging with a nanoplasmonic probe capable of nanometer-scale spatial resolution. Although its geometry and composition differ from those of the numerically-studied probe mentioned above [23], this probe similarly avoids the trade-off between resolution and contrast by isolating the light-coupling aperture from the

#145386 - $15.00 USD Received 5 Apr 2011; revised 13 May 2011; accepted 22 May 2011; published 25 May 2011

sensing location. As illustrated in Fig. 1, near-field light from a sample surface is captured by the enhanced electromagnetic interaction at the sharp apex of an atomic force microscope (AFM) probe. The light is guided along the ridge of the pyramidal tip as an SP wave. At the base of the pyramid, a large aperture (with a diameter on the order of half a wavelength) located adjacent to one vertex couples the light into the far field. The location of this aperture adjacent to the base rather than at the apex of the pyramidal tip allows the interactions of the tip with the sample to be localized on a scale comparable to the apex radius of curvature without sacrificing optical throughput. We will refer to this probe as the nanoplasmonic offset-aperture (NOA) probe. Notably, this NOA probe does not require alteration of the AFM probe apex and hence allows for simultaneous mapping of electromagnetic energy (by NSOM) and topography (by AFM) with resolution that is limited only by the sharpness of the probe's apex.

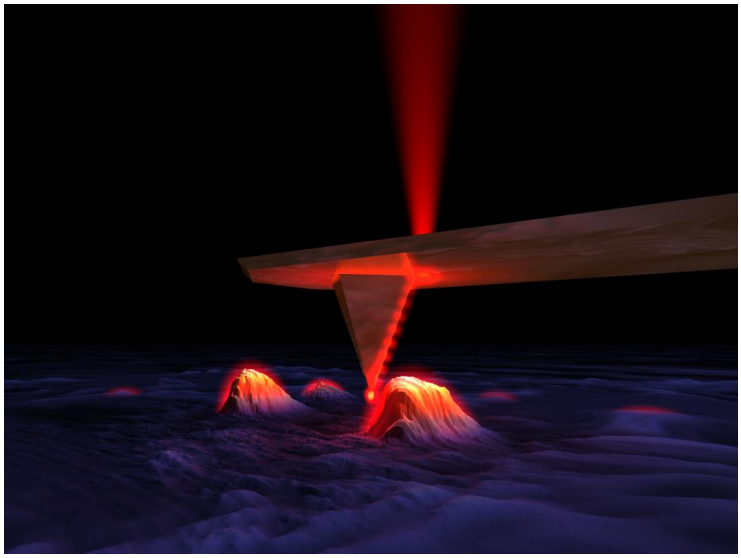

Fig. 1. Illustration of the collection-mode operation of a nanoplasmonic offset-aperture (NOA) probe.

2. Experimental setup

We have demonstrated the operation of the NOA probe in a collection mode configuration: the nanostructure was illuminated with far-field light, the probe interacted with the optical near field of the sample, and SP waves coupled to the probe and were scattered through the offset aperture.

To fabricate the NOA probe, a contact-mode silicon dioxide AFM probe (with a resonant frequency of 10 kHz, a width of 53 μm, and a length of 444 μm) was sputter-coated on its tip side with a 2 nm Cr adhesion layer followed by a 57 nm Au layer. The offset aperture (660 nm in diameter) was milled through the 1.5 μm-thick probe cantilever adjacent to one ridge of the pyramidal tip using a focused ion beam (FIB). The inset of Fig. 2 shows the AFM tip with the small offset aperture in close proximity to one corner of the pyramid. In this configuration, the ridge that acted to guide the SP waves from the pyramid apex to the aperture was 16 μm long. The material removed for the aperture was considered to be negligible: the mechanical resonance of the probe cantilever was not significantly affected and the probe still functioned normally. The radius of the tip apex was nominally less than 10 nm; however, many scans were performed during alignment of the system before near-field images were successfully obtained. After approximately 1000 scans, the sharpness of the tip degraded to a radius of 125 nm (as shown in Fig. 3). This degradation was expected to limit the spatial resolution of the topographical images.

#145386 - $15.00 USD Received 5 Apr 2011; revised 13 May 2011; accepted 22 May 2011; published 25 May 2011

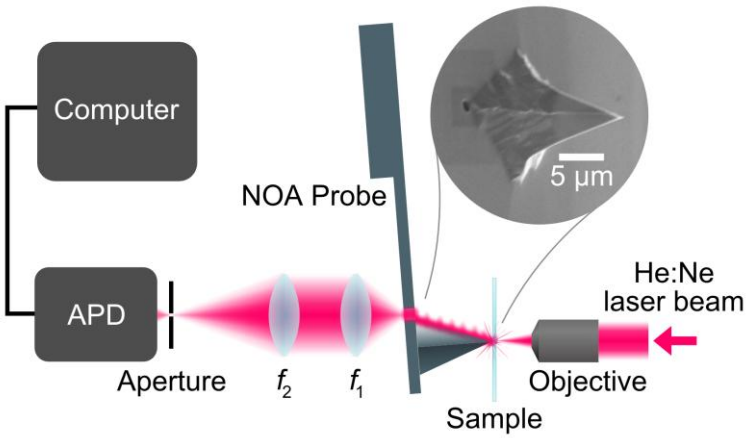

Fig. 2. Schematic diagram of the collection-mode near-field optical imaging system. NOA probe: nanoplasmonic offset-aperture probe; APD: avalanche photodiode. Inset: scanning electron micrograph of the NOA probe before any scanning was performed.

To acquire near-field images, the NOA probe was mounted in a commercial AFM system and positioned above a sample. The AFM was integrated with an inverted optical microscope. Figure 2 depicts the optical setup for this NSOM instrument. The nanostructure of interest was illuminated by a helium-neon laser source (λ = 632.8 nm, 4 mW). A microscope objective (100 × , 1.25 NA, oil immersion) was used to focus the laser beam onto the underside of the nanostructure, which was situated on a microscope cover slip of thickness 280 μm. The optical signal from the near-field was collected above the probe by a confocal two-lens system (focal lengths f_1: f_2 = 3.25, yielding a magnification $M = 8.33$), such that light originating from the top surface of the probe cantilever was focused onto the plane of a pinhole aperture 100 μm in diameter. A silicon avalanche photodiode (APD) was placed immediately behind the pinhole. The pinhole aperture acted as a spatial filter for the APD, passing only the light collected from the focal plane of the f_1 lens and from within a circle approximately 12 μm in diameter centered on the offset aperture.

Since light of wavelength 632.8 nm was used to illuminate the sample, it should be noted the offset aperture was not actually subwavelength in size. Thus, far-field light scattered from the sample may have passed through the aperture, increasing the amount of optical noise in the detected signal. However, the confocal lens pair and spatial filter were expected to eliminate most of this noise, as the light did not originate from the focal plane of the f_1 lens.

3. Results

A demonstration of the optical and topographical imaging capabilities of the NOA probe is shown in Fig. 4. Here, clusters of gold nanoparticles are shown in simultaneously acquired AFM and NSOM images (Figs. 4(a) and 4(b), respectively). Evident in both images are two distinctive and almost identical features. From the topographical image, the radius of the left cluster is approximately 370 nm and the maximum height is about 300 nm. Since the radius of curvature of the probe apex (from Fig. 3) is comparable to this height, this sample is a good candidate for testing the resolution capabilities of the probe. In the near-field optical image,

#145386 - $15.00 USD Received 5 Apr 2011; revised 13 May 2011; accepted 22 May 2011; published 25 May 2011

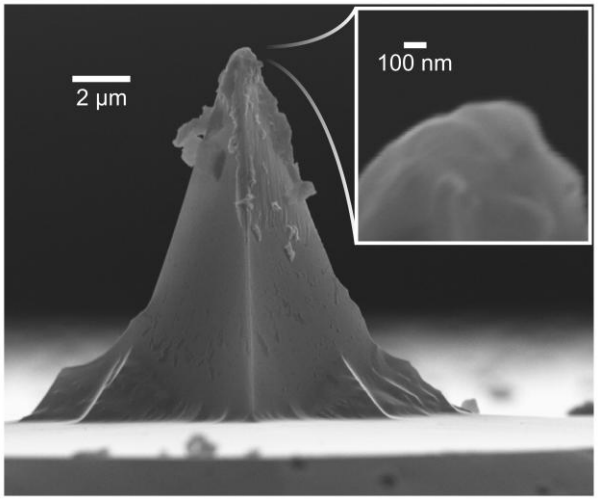

Fig. 3. Scanning electron micrograph of the nanoplasmonic offset-aperture probe after approximately 1000 scans. Inset: Apex of the tip shown at a higher magnification. The highest protrusion at the apex had a radius of curvature of 125 nm from this perspective.

the bright spots represent areas of increased optical coupling between the NOA probe and the clusters. A line profile (Fig. 4(c)) of the image taken at the left edge of the left cluster shows the resolution of the near field image to be 71 nm (using the 10%–90% criterion), while the resolution of the topographical image (by the same criterion) is 227 nm. Interestingly, the fine nanoscale features present in the background of the near-field image appear also in the topographical AFM image, suggesting a better resolution could be observed if a scan was performed at a higher spatial magnification. A gold film sample was scanned at a higher magnification in an attempt to explore the resolution limit of the NOA probe. An example image is shown in Fig. 5. Here, a nanostructure near the edge of the gold film was imaged, again simultaneously by AFM and NSOM (Fig. 5(a) and Fig. 5(b), respectively). A distinctive polygonal structure is revealed by both techniques. A line profile taken of the bottom edge of the structure shows the resolution of the optical image to be 45 nm, corresponding to $\lambda/14$ for helium-neon laser light. The same feature shows a resolution of 112 nm in the topographical image.

4. Discussion

A close examination of the experimental results raises important issues. As mentioned previously, the topographical and optical resolutions of the NOA probe were found to differ significantly. In addition, the optical images of the two samples showed an intriguing difference: The topographically highest points for the nanoparticle sample (Fig. 4) were locations where larger amounts of light coupled to the NOA probe ("bright" regions), while the topographically highest points for the bulk gold sample (Fig. 5) were locations where relatively small amounts of light coupled to the NOA probe ("dark" regions). Also visible are subtle directional artifacts in both the optical and topographical images. Signal strength and sources of noise are important to consider in these image analyses. In light of these points, the validity of the claimed resolution of this instrument will be discussed.

4.1 Imaging mechanism

The differences between the optical and topographical images of Figs. 4 and 5 can be understood in terms of the different mechanisms by which the images are formed. Atomic force topographical images are formed as a result of electrostatic repulsion and attraction between the probe and the sample, while the near-field optical images are formed as a result

#145386 - $15.00 USD Received 5 Apr 2011; revised 13 May 2011; accepted 22 May 2011; published 25 May 2011

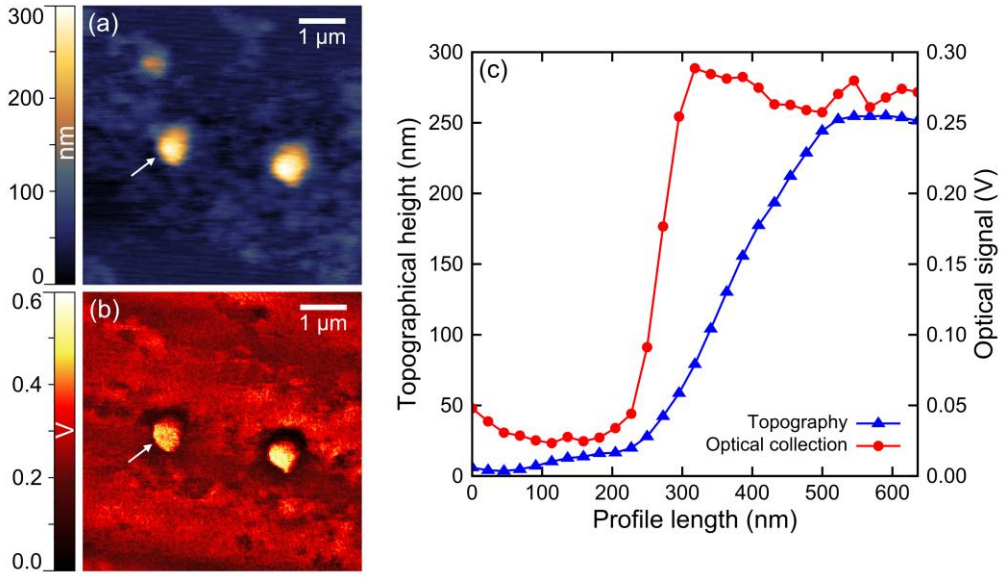

Fig. 4. Images acquired with the nanoplasmonic offset-aperture probe, showing clusters of 30 nm Au nanoparticles. (a) Contact-force topography. (b) Near-field optical collection. (c) Averaged line profiles taken from the same area in each image (as indicated by the arrows). These line profiles display a 10%–90% criterion resolution of 227 nm for the topographical image and 71 nm for the optical image. The zero points for both signal voltage and height were selected based on the lowest values present in the data.

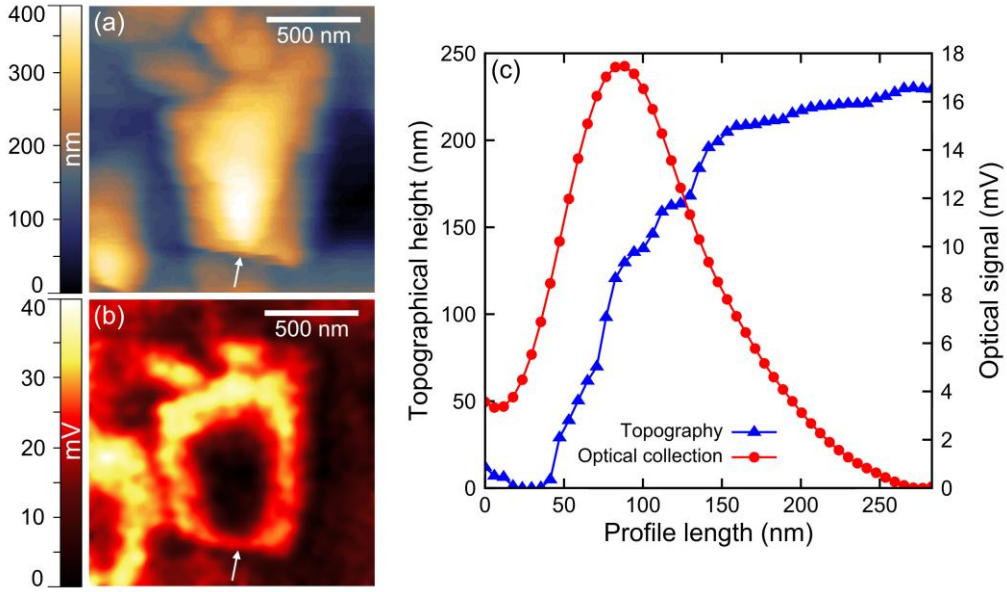

Fig. 5. Images acquired with the nanoplasmonic offset-aperture probe, showing a gold nanostructure. (a) Contact-force topography. (b) Near-field optical collection. (c) Averaged line profiles taken from the same area in each image (as indicated by the arrows). These line profiles display a 10%–90% criterion resolution of 112 nm for the topographical image and 45 nm for the optical image (on the rising edge of the peak). The zero points for both signal voltage and height were selected based on the lowest values present in the data.

#145386 - $15.00 USD Received 5 Apr 2011; revised 13 May 2011; accepted 22 May 2011; published 25 May 2011

of electromagnetic interactions between the probe and the sample. The electromagnetic interactions (of optical wavelengths) are strongly enhanced by the region of the probe with the smallest radius of curvature, principally the tip apex, while the electrostatic interactions are not enhanced to the same degree. Thus, while the topographical signal can result from contact of any part of the probe with the sample surface, the coupling of near-field optical energy takes place only at the very apex of the probe tip. This is the primary mechanism by which the optical images display a better resolution than the topographical images. As further evidence for this proposed mechanism, consider the effects of the differing composition of the two samples of Figs. 4 and 5. The sample imaged in Fig. 4 was composed of gold nanoparticles, while the sample imaged in Fig. 5 was composed of bulk gold. As illustrated in Fig. 6, these differing compositions resulted in the topographically highest points of the nanoparticle sample appearing as dark regions. As the probe approached the nanoparticle sample (Fig. 6(b)), its apex was in contact with the substrate glass and small numbers of gold nanoparticles, resulting in a moderately strong signal that propagated to the probe aperture and ultimately to the detector. However, as the probe climbed the steep nanoparticle cluster (Fig. 6(c)), the tip apex was far from any surface and only the side of the probe was in contact with the cluster. The resultant coupling was very weak, yielding a dark area in the near-field optical image. As the probe neared the top of the cluster (Fig. 6(d)), coupling strength increased since the apex came into optical contact with the cluster. This strong coupling was maintained on top of the cluster (Fig. 6(e)) because the nanoparticles couple light between and among each other through the interior of the cluster to its surface, despite the cluster's apparent thickness. In contrast, light strongly couples to the edges of the bulk gold nanostructure, but will not transmit through the material for thicknesses much greater than the skin depth (which is approximately 31 nm for light of wavelength 632.8 nm [24]). The surface waves excited at the edge decay at a finite distance from the edge, leaving the center of the nanostructure dark (Fig. 6(j)). The result is an apparent edge enhancement in the near-field optical image of Fig. 5, as the strongest signal only occurs where the probe apex is in contact with the nanostructure but not too far from the nanostructure's edge (Fig. 6(i)). If the strength of the optical coupling depended only on the amount of probe surface area in contact with the sample, for instance, we would not have observed bright centers for the nanoparticle clusters of Fig. 4. Thus, optical coupling must take place preferentially at the very apex of the probe.

4.2 Probe asymmetry

Noticeable in the optical images of Figs. 4 and 5 are subtle directional artifacts that are not present in the corresponding topographical images. (Artifacts which appear in both images, such as the visual smearing of the sides of the polygonal nanostructure in Fig. 5(a), are due to the degraded probe apex.) These artifacts are caused by the inherent asymmetry of our design for the NOA probe: there is only one aperture, located at the end of one ridge of the pyramidal tip. Due to the orientation of the probe with respect to the sample as shown in Figs. 6(a) and 6(f), this asymmetry results in an apparent brightening of areas to the lower left of the observed nanostructures, and an apparent darkening of areas to the upper right of the observed nanostructures. In both cases the tip apex is too far from any surface to couple light efficiently, and the brightening corresponds to instances where the tip ridge feeding the aperture is coupling light from the nanostructure, while the darkening corresponds to instances where the tip ridge opposite the aperture is coupling light from the nanostructure. See Fig. 7 for an illustration of this mechanism. These directional artifacts may be avoided in the future by designing NOA probes with multiple apertures that are distributed symmetrically with respect to the probe tip. For example, one could include a circular aperture for each of the four ridges of the pyramidal tip.

#145386 - $15.00 USD Received 5 Apr 2011; revised 13 May 2011; accepted 22 May 2011; published 25 May 2011

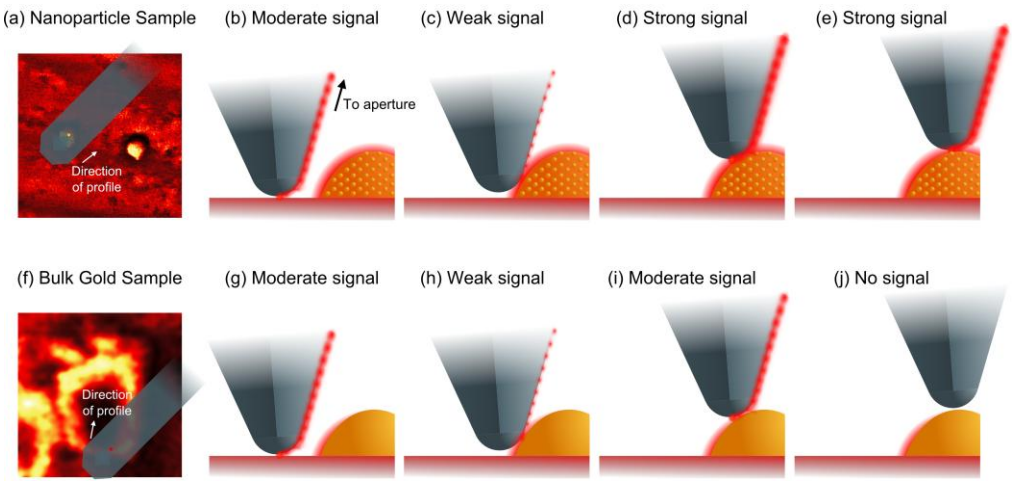

Fig. 6. Overview of an imaging mechanism that is consistent with the experimental results presented for the nanoplasmonic offset-aperture (NOA) probe. The upper panels of this figure depict a sequence of events which allowed formation of the image shown in Fig. 4(b). The lower panels depict a similar sequence of events which allowed the formation of the image shown in Fig. 5(b). (a) The orientation of the probe with respect to the image as acquired is shown (not to scale). The arrow indicates the direction of the line profile shown in Fig. 4(c), taken from the shown location of the probe tip. (b) The probe tip is in contact with the substrate, mediated by small numbers of nanoparticles (not shown); a moderately strong optical signal is detected. (c) The probe tip is far from any surface, while the tip side is in contact with the sample; a weak signal is detected. (d) The probe tip nears the top of the nanoparticle cluster; a strong signal is detected. (e) The probe tip is atop the nanoparticle cluster; a strong signal is detected. (f) As in (a), the orientation and location of the probe (not to scale) and the direction of the line profile from this location are indicated, but for the bulk gold sample of Fig. 5. (g) The probe tip is in contact with the substrate, mediated by small amounts of bulk gold (not shown); a moderately strong signal is detected. (h) The probe tip is far from any surface, while the tip side is in contact with the sample; a weak signal is detected. (i) The probe tip nears the top of the bulk gold sample; a moderate signal is detected. (j) The probe tip is atop the bulk gold sample; no signal is detected.

4.3 Signal strength and optical noise

The bulk of the optical noise present in the images of Figs. 4 and 5 was expected to originate from far-field light scattered by the components of the optical system. As mentioned in Section 2, far-field light scattering from the sample through the probe aperture was not a significant component of this noise, since it was spatially filtered by the lenses and pinhole aperture between the probe and the APD. Much of the optical noise was the result of far-field light scattering off the back side of the probe in the vicinity of the probe aperture, which would have been collected from the focal plane of the f_1 lens and passed through the spatial filter.

It is possible that use of the NOA probe in an illumination-mode configuration (where light is coupled through the probe aperture and allowed to interact with the sample only at the tip apex) would have eliminated this noise source. However, the large aperture of the NOA probe used in this experiment would have allowed a significant amount of far-field light through the cantilever. This light would have scattered off the sample in the vicinity of the probe tip, drowning out the near-field optical signal. Since far-field light passing through the aperture does not significantly affect collection-mode measurements, and the larger aperture enhances the coupling of the near-field optical signal into the far field, the probe used in this experiment (which had an aperture diameter slightly larger than λ) was better suited to collection-mode operation. NOA probes for use in illumination mode should be fabricated with an aperture diameter of approximately $\lambda/2$ to reduce leakage of far-field light through the aperture [22]. The rejection of optical noise could be improved in future experiments with the

#145386 - $15.00 USD Received 5 Apr 2011; revised 13 May 2011; accepted 22 May 2011; published 25 May 2011

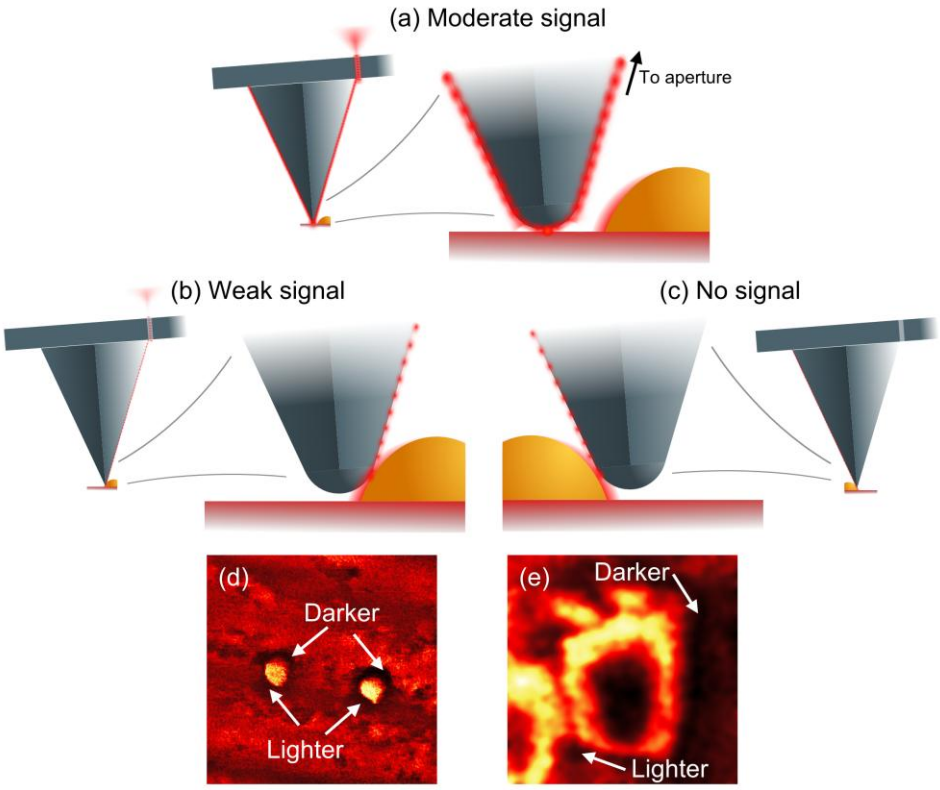

Fig. 7. The inherent asymmetry of the nanoplasmonic offset-aperture (NOA) probe leads to slight directional artifacts in the optical images. (a) Despite the depiction in Fig. 6, light coupling from the sample to the probe apex propagates up the entire surface of the pyramidal tip. However, only light propagating on the ridge adjacent to the aperture will be coupled into the far field and detected. (This ridge is indicated by the arrow and label.) (b) As in Fig. 6(h), the probe is in contact with the edge of a gold nanostructure. The apex is too far from any surface to couple light efficiently, and the side of the probe adjacent to the aperture couples light weakly. (c) The probe is in contact with the opposite side of the same nanostructure depicted in (b). Again, the apex does not couple efficiently, and the side of the probe couples light weakly. However, the side which couples is opposite the aperture, and no light is guided to the aperture. (d,e) The mechanism illustrated by (a) through (c) explains the observed directional artifacts in the optical images obtained. The areas to the lower left of each nanostructure tend to be brighter than the areas to their upper right. The mechanism of (b) takes place to the lower left; the mechanism of (c) takes place to the upper right. Note that the probe is oriented relative to the sample as indicated in Figs. 6(a) and 6(f).

NOA probe by modulation of the tip–sample distance and lock-in detection of the optical signal. Unfortunately, this option was not available for our AFM instrument. Conversely, it could be perceived as an advantage of the NOA probe that lock-in techniques are not required to achieve near-field optical imaging.

Another way to reduce the effect of noise on the measurement would be to increase the signal strength. To reach the aperture, SP waves from the tip apex must propagate approximately 16 μm along one ridge of the pyramidal tip. This ridge acts similarly to a metallic (silver) wedge waveguide with a wedge angle of approximately 100 degrees, for which the propagation loss is 0.23 dB/μm [25]. This gives a 1/*e* propagation distance of 19 μm. Although the losses will be slightly greater for a gold wedge waveguide, this calculation demonstrates that the SP wave losses along the ridge of the tip were reasonable for this experiment. Additionally, the optical signal leaving the aperture could be made significantly stronger through the use of a NOA probe with a shorter tip ridge.

#145386 - $15.00 USD Received 5 Apr 2011; revised 13 May 2011; accepted 22 May 2011; published 25 May 2011

4.4 Spatial resolution

In an instrument such as this one, where a single probe provides two distinct types of data, the concept of spatial resolution can become ambiguous. Figures 4(c) and 5(c) offer a direct comparison between topographical and optical line profiles, and this is not intended to be misleading. It is easy to take for granted that the spatial resolution should be defined as the NOA probe's ability to render the "true object" present on the sample slide. In applying the well-accepted 10%–90% criterion to the data of Figs. 4(c) and 5(c), we can see that the near-field optical data set rises faster per-nanometer than the atomic force topographical data set, and it is easy to conclude from this that the near-field optical image must then be a better representation of the true object. However, this would not be entirely correct, as the object measured is different in each case: the optical signal detected by the APD measures the interaction between the tip apex and the electromagnetic near-field of the nanostructure, while the cantilever deflection detected by the AFM measures the electrostatic interactions between the atoms of the tip surface and the atoms of the sample surface. Therefore, each measurement provides different information about the nanostructure in question.

However, this does not change our conclusion that a finer probing tip (e.g. without wear from extended use) would allow acquisition of both optical and topographical images with better resolution than was measured for this paper: The descriptions of the proposed imaging mechanisms illustrate that both the optical and topographical imaging resolutions depend strongly on the radius of curvature of the tip apex. Additionally, improvements to the NOA probe design discussed here would reduce imaging artifacts and increase confidence in future resolution measurements. Investigators with inexpensive access to FIB tools may be able to explore the true limits of the NOA probe design by fabricating and testing new probes.

5. Conclusions

By spatially isolating the light-coupling aperture from the light-localizing structure, the nanoplasmonic probe demonstrated here can provide excellent spatial resolution for near-field optical imaging while also allowing high-resolution atomic force topographical imaging. The spatial resolution of the optical images was about three times better than the spatial resolution of the topographical images. Although it is important to remember that each imaging technique measures fundamentally different phenomena, an NOA probe having a sharper apex would yield images of higher resolution for both techniques. Since the NOA probe can be integrated both with conventional AFM and NSOM instruments, this design has the potential to become a viable alternative to the hollow-pyramid-type apertured probes common in commercial NSOM instruments. The relative simplicity of fabricating these probes will also reduce the cost of NSOM systems significantly.

Acknowledgments

The authors acknowledge valuable discussions with Dr. Michele Celebrano of ETH Zürich. This work was supported by the Natural Sciences and Engineering Research Council of Canada (NSERC) and the Canada Research Chairs (CRC) program of the Government of Canada.

#145386 - $15.00 USD Received 5 Apr 2011; revised 13 May 2011; accepted 22 May 2011; published 25 May 2011